



# CHORUS

This is the accepted manuscript made available via CHORUS. The article has been published as:

## $^3\text{He}$ - $^{129}\text{Xe}$ Comagnetometry using $^{87}\text{Rb}$ Detection and Decoupling

M. E. Limes, D. Sheng, and M. V. Romalis

Phys. Rev. Lett. **120**, 033401 — Published 16 January 2018

DOI: [10.1103/PhysRevLett.120.033401](https://doi.org/10.1103/PhysRevLett.120.033401)

# $^3\text{He}$ - $^{129}\text{Xe}$ Comagnetometry using $^{87}\text{Rb}$ Detection and Decoupling

M. E. Limes, D. Sheng, and M. V. Romalis

Department of Physics, Princeton University, Princeton, New Jersey, 08544, USA

(Dated: December 6, 2017)

We describe a  $^3\text{He}$ - $^{129}\text{Xe}$  comagnetometer using  $^{87}\text{Rb}$  atoms for noble-gas spin polarization and detection. We use a train of  $^{87}\text{Rb}$   $\pi$  pulses and  $\sigma^+/\sigma^-$  optical pumping to realize a finite-field Rb magnetometer with suppression of spin-exchange relaxation. We suppress frequency shifts from polarized Rb by measuring the  $^3\text{He}$  and  $^{129}\text{Xe}$  spin precession frequencies in the dark, while applying  $\pi$  pulses along two directions to depolarize Rb atoms. The plane of the  $\pi$  pulses is rotated to suppress the Bloch-Siegert shifts for the nuclear spins. We measure the ratio of  $^3\text{He}$  to  $^{129}\text{Xe}$  spin precession frequencies with sufficient absolute accuracy to resolve the Earth's rotation without changing the orientation of the comagnetometer. A frequency resolution of 7 nHz is achieved after integration for 8 hours without evidence of significant drift.

PACS numbers: 32.30.Dx, 06.30.Gv, 39.90.+d

Spin comagnetometers first introduced in [1] are used for several types of fundamental physics experiments, such as tests of Lorentz, CP and CPT symmetries [2–5] and searches for spin-dependent forces [6–10]. They also have practical applications as inertial rotation sensors [11–16]. When two different spin ensembles occupy the same volume they experience nearly the same average magnetic field [17]. The ratio of their spin precession frequencies  $f_r = \omega_{\text{He}}/\omega_{\text{Xe}}$  can then be used to measure the inertial rotation rate  $\Omega$  or a spin coupling beyond the Standard Model  $b$ :

$$f_r = (\gamma_{\text{He}}B_0 + \Omega_z + b_z^{\text{He}})/(\gamma_{\text{Xe}}B_0 + \Omega_z + b_z^{\text{Xe}}). \quad (1)$$

where  $B_0$  is the bias field along  $\hat{z}$  and  $\gamma_{\text{He}}$ ,  $\gamma_{\text{Xe}}$  are the gyromagnetic ratios for  $^3\text{He}$  and  $^{129}\text{Xe}$ , which are well known [18]. Since  $I = 1/2$  nuclear spins are free from quadrupolar energy shifts [19],  $f_r$  provides an absolute measure of non-magnetic spin interactions—this is particularly important in searches for spin-gravity coupling [20] (where the interaction is hard to modulate), and for use as a gyroscope.

An alkali-metal magnetometer provides a natural way to detect nuclear-spin signals because Rb atoms are already used to polarize the nuclear spins by spin-exchange collisions; these collisions enhance the classical dipolar field from the nuclear magnetization by a factor  $\kappa_0$  [21], which is about 5 for Rb- $^3\text{He}$  [22] and 500 for Rb-Xe [23]. However, the presence of polarized Rb atoms also causes large noble-gas frequency shifts that affect the accuracy of Eq. (1). In the past, these frequency shifts have been avoided in  $^3\text{He}$ - $^{129}\text{Xe}$  comagnetometers by detecting a smaller dipolar field outside of an alkali-free cell using an RF coil [24] or a SQUID magnetometer [25].

In this Letter we describe a new method for operating the  $^3\text{He}$ - $^{129}\text{Xe}$  comagnetometer using  $^{87}\text{Rb}$  readout with high sensitivity and accuracy. We develop a  $^{87}\text{Rb}$  magnetometer that can operate in a finite magnetic field of about 5 mG while suppressing Rb-Rb spin-exchange relaxation to increase the magnetometer sensitivity. It

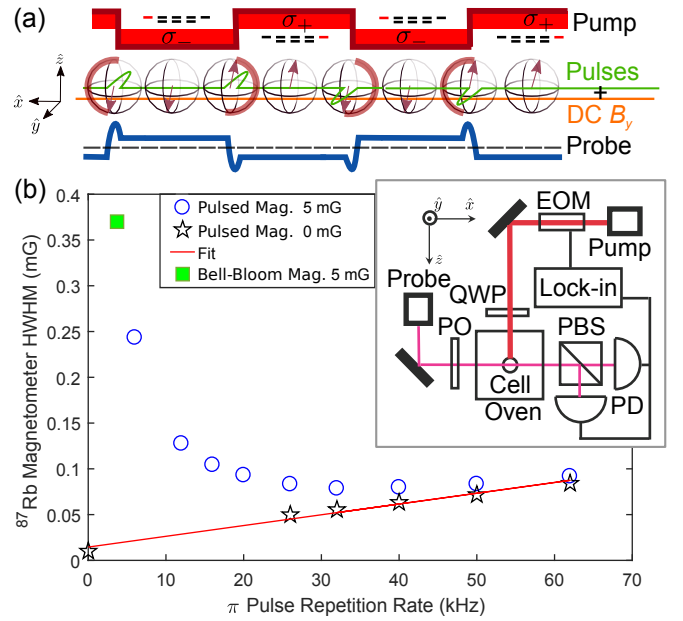


FIG. 1. (a) The pulse-train  $^{87}\text{Rb}$  magnetometer uses  $\hat{y}$ -axis  $\pi$  pulses with a  $\sigma^+/\sigma^-$  pump beam along  $\hat{z}$  and a linearly polarized probe beam along  $\hat{x}$  (see inset). A  $B_y$  field gives a paramagnetic Faraday rotation signal detected with a lock-in. (b) Using a  $^{87}\text{Rb}$ - $\text{N}_2$  cell at  $103^\circ\text{C}$  and low laser power, we measure the magnetometer linewidth in zero bias field (stars) and for  $B_0 = 5$  mG (circles) as a function of  $\pi$  pulse repetition rate. For comparison we also show a Bell-Bloom magnetometer linewidth (square) that is limited by Rb-Rb spin-exchange relaxation.

uses a train of  $^{87}\text{Rb}$   $\pi$  pulses in unison with  $\sigma^+/\sigma^-$ -modulated optical pumping to refocus spin precession of  $^{87}\text{Rb}$  in the  $B_0$  field, while retaining sensitivity to transverse fields (see Fig. 1a). To suppress nuclear-spin frequency shifts we use a Ramsey pump-probe sequence where the  $^3\text{He}$  and  $^{129}\text{Xe}$  frequencies are measured in the absence of Rb laser light [17]. In addition, we suppress back-polarization of Rb due to noble gases by a factor of

$10^3$  using a train of  $^{87}\text{Rb}$   $\pi$  pulses along both  $\hat{x}$  and  $\hat{y}$  directions. Finally, we show that the effect of the  $^{87}\text{Rb}$   $\pi$  pulses on the ratio of the noble gas frequencies can be eliminated by rotating the plane of the pulses about the  $\hat{z}$  axis at the sum of the  $^3\text{He}$  and  $^{129}\text{Xe}$  spin precession frequencies. Using this method and Eq. (1) we can measure the Earth's rotation without changing the orientation of the magnetometer, in contrast to previous measurements that required physical rotation of the apparatus to modulate the signal [5].

*Pulse-train Alkali Magnetometer.*— The effect of  $^{87}\text{Rb}$   $\pi$  pulses can be understood by considering precession about  $B_0$  of the  $F_a = I + 1/2$  and  $F_b = I - 1/2$   $^{87}\text{Rb}$  spin manifolds, which have opposite gyromagnetic ratios  $\pm\gamma_{\text{Rb}}$  [26]. After a  $\pi$  pulse, the relative orientation of  $\langle \mathbf{F}_a \rangle$  and  $\langle \mathbf{F}_b \rangle$  remains the same. If the time  $\tau$  between  $\pi$  pulses along  $\hat{y}$  is small,  $\tau \ll (\gamma_{\text{Rb}} B_0)^{-1}$ , the spin evolution due to  $B_0$  is cancelled to first order. Thus, the magnetometer effectively operates at zero magnetic field in the spin-exchange relaxation free (SERF) regime [27]. The only limitation comes from the finite duration of the  $\pi$  pulses,  $t_p$ , during which spin-exchange relaxation occurs. As shown in [28], the remaining relaxation rate is proportional to the duty cycle of the pulses  $t_p/\tau$ .

To demonstrate spin-exchange suppression in the pulse-train  $^{87}\text{Rb}$  magnetometer we use a  $^{87}\text{Rb}$ - $\text{N}_2$  cell. The cell is heated in a boron nitride oven by AC currents and is located inside five cylindrical  $\mu$ -metal shields. We use two sets of field coils, a larger set to provide the bias field and a smaller set of three-axis square Helmholtz coils for  $^{87}\text{Rb}$  tipping pulses (3.5 in. side, two turns,  $3 \mu\text{H}$ ). The  $^{87}\text{Rb}$   $\pi$  pulses (following sequence  $\pi_y \pi_y \pi_{-y} \pi_{-y}$ ) are typically 1.5-3  $\mu\text{s}$  in duration and 1-2 A in amplitude. They are generated with a pulsed current source using an LT1210 driver with an LC filter at the output to eliminate any DC currents in the coil.

In Fig. 1b we show measurements of the magnetic resonance linewidth for a  $B_y$  field magnetometer signal. When the bias field  $B_0 = 0$ , the geometry matches a SERF magnetometer. The resonance linewidth increases linearly with the duty cycle of the  $\pi$  pulses. When  $B_0 = 5$  mG, the linewidth drops as the  $\pi$  pulse rate increases, a result of canceling the precession of  $\langle \mathbf{F}_a \rangle$  and  $\langle \mathbf{F}_b \rangle$  away from each other due to the  $B_0$  field. Simultaneously, the amplitude of response to a  $B_y$  field increases [29]. Finally, we show the linewidth for a Bell-Bloom magnetometer, where  $\sigma^+/\sigma^-$  polarization is modulated at the  $^{87}\text{Rb}$  Larmor frequency (3.7 kHz) and the magnetometer signal corresponds to a change in  $B_z$  field. This provides a measure of the spin-exchange-limited linewidth in our bias field, and demonstrates that our pulse train reduces the linewidth by a factor of 5.

In the presence of the noble gases, the pulse-train magnetometer provides additional advantages. It maintains zero average  $^{87}\text{Rb}$  polarization to minimize noble-gas frequency shifts. If the pump laser is turned off, it actively

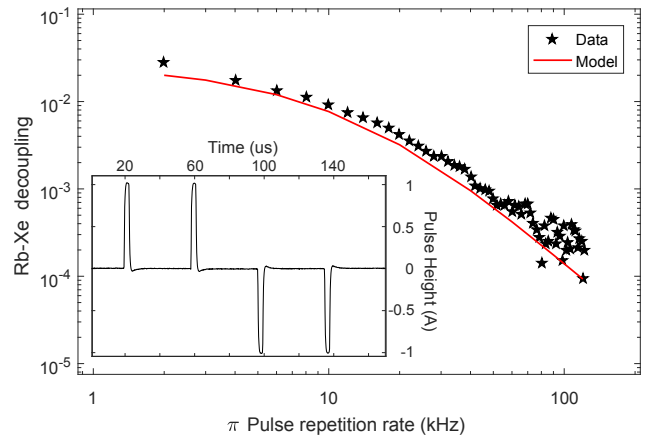


FIG. 2. The Rb back polarization from spin exchange with  $^{129}\text{Xe}$  is reduced by a factor of  $10^4$  by increasing the pulse repetition rate, in agreement with predictions from a Rb density matrix model including Rb-Rb spin-exchange. The inset shows the current flowing through the coil to generate typical  $\pi$  pulses.

depolarizes Rb atoms from back-polarization created by polarized  $^{129}\text{Xe}$ . Fig. 2 shows the fraction of  $^{87}\text{Rb}$  back-polarization that remains in the presence of the pulses. This data was obtained by first polarizing  $^{129}\text{Xe}$  along the bias field, then shuttering the pump light and monitoring  $^{87}\text{Rb}$  back-polarization along the bias field using Faraday rotation, while periodically reversing  $^{129}\text{Xe}$  spins [29]. We realize a depolarization factor of  $10^4$ , about 2 orders of magnitude larger than was achieved using a continuous RF field resonant with  $^{87}\text{Rb}$  atoms in [17].

*Noble-Gas Comagnetometer.*— The  $^3\text{He}$ - $^{129}\text{Xe}$  comagnetometer uses a  $0.5 \text{ cm}^3$  spherical cell made from GE180 glass, with 9.3 atm  $^3\text{He}$ , 2.9 torr  $^{129}\text{Xe}$ , 40 torr  $\text{N}_2$ , and a droplet of enriched  $^{87}\text{Rb}$  that plugs the cell stem. In this cell the magnetic linewidth is about 0.5 mG for optimized intensity of pump and probe lasers, due to additional broadening by Rb-Xe spin-destruction collisions. The magnetic field sensitivity of the pulse-train  $^{87}\text{Rb}$  magnetometer is  $40 \text{ fT}/\sqrt{\text{Hz}}$  [29]. The nuclear-spin relaxation time due to wall collisions is about  $10^3$  s for  $^{129}\text{Xe}$  and much longer for  $^3\text{He}$ . At the operating temperature of 110-120°C the  $^{129}\text{Xe}$  spin relaxation time is about 200 s, limited by Rb-Xe spin-exchange collisions.

The comagnetometer is operated in a pump-probe cycle. First  $^3\text{He}$  and  $^{129}\text{Xe}$  are polarized along  $B_0$ . We start the sequence for pulse-train  $^{87}\text{Rb}$  magnetometry and, using large field coils, apply a noble-gas tipping pulse that places both  $^3\text{He}$  and  $^{129}\text{Xe}$  in the plane transverse to the bias field [29]. The tipping angle for  $^3\text{He}$  and  $^{129}\text{Xe}$  is crucial for accurate comagnetometry due to long-range dipolar fields generated by the noble gases in the imperfectly spherical cell [29]. However, dipolar fields do not cause a significant frequency shift if the nuclear-

spin polarization is exactly orthogonal to  $B_0$  and remains so throughout the measurement. It is important to tune the pump laser exactly to the D1 resonance, as the  $^{87}\text{Rb}$  pump light-shift can cause tipping of nuclear spins during the measurement. The precession signals from  $^3\text{He}$  and  $^{129}\text{Xe}$  are on the order of 0.3 mG; we limit the amplitudes to less than the magnetometer linewidth to avoid large non-linearities.

The nuclear-spin precession measurements can be performed continuously with the pulse-train  $^{87}\text{Rb}$  magnetometer. However, we find the noble-gas long-term frequency stability is insufficient with this method because the  $\hat{y}$  pulse train allows back-polarization of  $^{87}\text{Rb}$  along the  $\hat{y}$  axis [29]. Therefore, we apply two-axis depolarization using the pulse sequence  $\pi_y\pi_x\pi_y\pi_x\pi_x\pi_y\pi_x\pi_y\pi_x$ . This prevents continuous use of the  $^{87}\text{Rb}$  magnetometer, so we use Ramsey-type ‘in-the-dark’ measurements. After an initial precession period, the pump and probe lasers are turned off with AOMs and mechanically shuttered, and the  $\hat{x}$   $^{87}\text{Rb}$   $\pi$  pulses are turned on, interspersing the  $\hat{y}$  pulses. After waiting about  $0.7 T_2^{\text{Xe}}$ , the pulse-train  $^{87}\text{Rb}$  magnetometer is used again to detect  $^3\text{He}$ - $^{129}\text{Xe}$  precession, see Fig. 3a. At the end of the precession measurement we coherently put the remaining nuclear polarization along (or against)  $B_0$  by sending the lock-in output to the  $\hat{x}$  coil, which yields out-of-phase on-resonance magnetic fields for both  $^3\text{He}$  and  $^{129}\text{Xe}$  [30, 31]. We then apply a magnetic field gradient to dephase any remaining transverse nuclear spin polarization. The noble gases are then polarized along  $B_0$  for about 20 s using full Rb polarization, and the cycle repeats.

We process the data by fitting each detection period to two decaying sine waves and extract the  $^3\text{He}$  and  $^{129}\text{Xe}$  zero-crossing times upon entering and exiting the dark period. We use the spin precession frequencies during the detection periods to find the integer number of precession periods between the zero-crossings in the dark. The  $^3\text{He}$ - $^{129}\text{Xe}$  polarization signals are large enough that the  $^{87}\text{Rb}$  magnetometer response becomes slightly non-linear, causing  $^3\text{He}$ - $^{129}\text{Xe}$  cross-modulation peaks. We correct for this effect by fitting with an expanded Lorentzian [29]. From zero crossing times we find the  $^3\text{He}$  and  $^{129}\text{Xe}$  ‘in-the-dark’ precession frequencies  $\omega_{\text{He}}$  and  $\omega_{\text{Xe}}$ , and the frequency ratio  $f_r$ . The rotation rate is given from Eq. (1),

$$\Omega_z = \omega_{\text{Xe}} \frac{\gamma_r - f_r}{(\gamma_r - 1)}, \quad (2)$$

where  $\gamma_r = \gamma_{\text{He}}/\gamma_{\text{Xe}}$ . In Fig. 3b we show the Allan deviation of successive measurements of  $\Omega_z$ . The scatter for successive spin precession cycles is typically about 70 nHz and the fit indicates an angle-random-walk of  $0.025 \text{ deg}/\sqrt{\text{hour}}$ .

The last step in suppressing noble-gas frequency shifts is to eliminate the effect of  $^{87}\text{Rb}$  depolarizing pulses. To

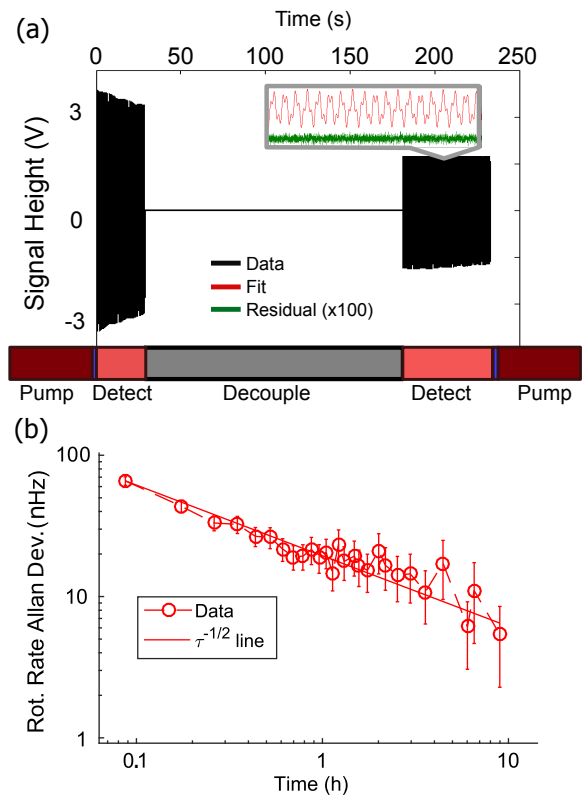


FIG. 3. (a) The Ramsey scheme with an inset showing a  $^3\text{He}$ - $^{129}\text{Xe}$  lock-in signal pattern and the fit residuals  $\times 100$ . (b) Allan deviation of the rotation rate  $\Omega_z$  with an 7 nHz ( $10^{-2}$  deg/hour) upper limit of the rotation rate stability.

analyze the effects of the pulses on the average nuclear-spin precession frequency we use average Hamiltonian theory (AHT) [29]. The  $\pi_y\pi_y\pi_x\pi_x\pi_y\pi_y$   $^{87}\text{Rb}$  magnetometer sequence produces a nuclear-spin frequency shift  $\omega_n = \gamma_n B_0 (1 - (\gamma_n B_1 t_p)^2/4)$ , accurate to third order in  $\gamma_n$  for sufficiently small pulse width  $t_p$ . The pulse field amplitude  $B_1$  is given by  $\gamma_{\text{Rb}} B_1 t_p = \pi$ , so the frequency shift is a multiplicative correction  $(\gamma_n \pi / \gamma_{\text{Rb}})^2/4 = 5.3 \times 10^{-5}$  for  $^3\text{He}$  and  $7 \times 10^{-6}$  for  $^{129}\text{Xe}$  frequencies. Finite pulse duration reduces the shifts by about 5%.

To eliminate these effects we introduce a novel technique of slowly rotating the plane of the pulses. For example, consider rotating the pulse train at a rate  $\omega_r$  that matches the  $^3\text{He}$  precession frequency—in the  $^3\text{He}$  rotating frame the  $B_0$  field is eliminated and the  $\pi$  pulses are the sole source of the magnetic field, so they produce no frequency shift if their time average is equal to zero. Experimentally this is achieved by applying current pulses to both  $x$  and  $y$  coils with amplitudes given by  $\cos(\omega_r)$  and  $\sin(\omega_r)$ . This technique works for any shape of the current pulses and is insensitive to first-order inaccuracies in their relative amplitudes and phase. However, there remains a sensitivity to the *planar* nature of the pulses, for example, the presence of metal strips near the cell generates eddy currents that cause an additional ap-

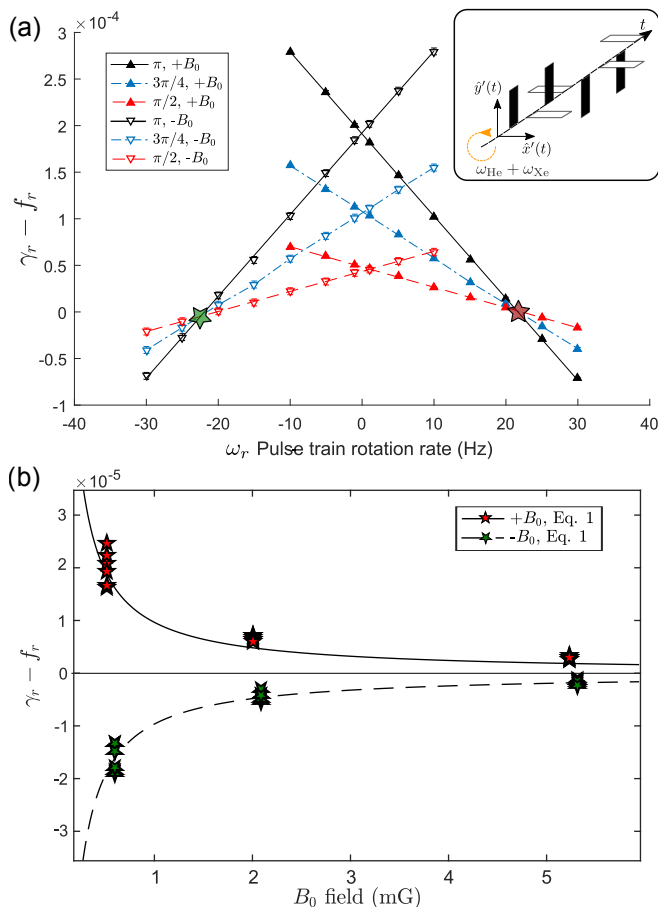


FIG. 4. (a) Frequency ratio  $f_r = \omega_{\text{He}}/\omega_{\text{Xe}}$  measured with  $^{87}\text{Rb}$  depolarizing  $\hat{x}$ - $\hat{y}$  pulse-train using  $\pi$ ,  $3\pi/4$ , and  $\pi/2$  pulses and rotating at frequency  $\omega_r$  for two directions of the bias magnetic field  $B_0 = 5.3$  mG. The stars show the intersection points where the effect of the pulses is cancelled. Inset: rotating  $\hat{x}$ - $\hat{y}$  pulse train. (b) Frequency ratio  $\omega_{\text{He}}/\omega_{\text{Xe}}$  at the intersection points (note a factor of 10 expanded vertical scale) as a function of  $B_0$ . Solid and dashed lines show prediction from Eq. 1 due to projection of Earth’s rotation on  $B_0$ .

parent rotation of the pulse field.

For the  $\pi_y \pi_x \pi_y \pi_x \pi_y \pi_x \pi_y \pi_x$  decoupling sequence applied during the in-the-dark period, AHT gives a frequency ratio of

$$f_r = \frac{\gamma_{\text{He}} B_0 + 3(\omega_r - \gamma_{\text{He}} B_0)(\gamma_{\text{He}} B_1 t_p)^2 / 8}{\gamma_{\text{Xe}} B_0 + 3(\omega_r - \gamma_{\text{Xe}} B_0)(\gamma_{\text{Xe}} B_1 t_p)^2 / 8}. \quad (3)$$

We find that  $f_r = \gamma_r$  for  $\omega_r = \omega_{\text{He}} + \omega_{\text{Xe}}$  and any  $B_1$ .

In Fig. 4a we show the measurements of the frequency ratio as a function of the rotation frequency  $\omega_r$  and  $B_1$  amplitude. We take data for both directions of  $B_0$  and reverse the direction of pulse rotation. The rotation frequency can be set to one of the intersection points, where  $f_r$  is independent of the amplitude of  $B_1$ , eliminating the shift due to pulses. It corresponds to the sum  $\omega_{\text{He}} + \omega_{\text{Xe}}$ , but can be slightly shifted if the pulses are not perfectly planar.

To check the accuracy of the comagnetometer, we measure the difference  $f_r - \gamma_r$  due to Earth’s rotation. We use  $\gamma_r = 2.7540813(3)$  from [18]. The chemical shift of  $^{129}\text{Xe}$  frequency due to He is estimated to be on the order of 0.2 ppm in our cell [32]. The data are shown in Fig. 4b as a function of  $B_0$ . The projection of the Earth’s rotation axis  $\Omega_{\text{E}}$  along the bias field is  $\Omega_z = \Omega_{\text{E}} \cdot \mathbf{B}_0 / B_0 = 6.5 \mu\text{Hz}$ . Although  $B_0$  is not parallel to the Earth’s rotation axis, the effect of Berry’s phase is negligible [33–36]. The predictions from Eq. (1) agree with our measurements without any frequency corrections, indicating absolute accuracy of frequency measurements at a level of about 1 ppm. Allan deviation measurements in Fig. 3 using the rotating decoupling field indicate that under stable experimental conditions the frequency stability is better 7 nHz or about 1 ppb. This corresponds to an upper limit on angular bias drift of 0.009 deg/hour.

In conclusion, we have developed techniques for operating a dual noble-gas comagnetometer with isotopes that have very different values of  $\kappa_0$  while using Rb vapor in the cell for polarization and detection of nuclear spins. We demonstrated a Rb magnetometry technique using  $\pi$  pulse trains that suppresses Rb-Rb spin-exchange relaxation in a finite magnetic field and maintains zero average Rb polarization. To further eliminate frequency shifts from polarized Rb we use a two-axis  $\pi$ -pulse train and make Ramsey-style measurements in the dark. By rotating these decoupling  $\pi$ -pulses we achieve sufficient absolute accuracy to measure Earth’s rotation without changing the comagnetometer orientation. We realize stability of 7 nHz after 8 hours, which is sufficient for detection of Planck-scale coupling of spins to Earth’s gravity [20]. The comagnetometer can also be used as a gyroscope with higher sensitivity and stability than previous nuclear-spin gyroscopes that use a  $^{129}\text{Xe}$ - $^{131}\text{Xe}$  combination with similar values of  $\kappa_0$  [16, 37]. The short-term sensitivity of our apparatus using a  $0.5 \text{ cm}^3$  cell is an order of magnitude better than for the  $^3\text{He}$ - $^{129}\text{Xe}$  spin maser [38] and similar to the SQUID-detected  $^3\text{He}$ - $^{129}\text{Xe}$  comagnetometer that has a 300 times larger cell volume [9]. The best short-term sensitivity we realized experimentally is  $0.01 \text{ deg}/\sqrt{\text{hour}}$ , while the Cramér-Rao frequency uncertainty lower bound based on the signal-to-noise ratio of the recorded  $^3\text{He}$  and  $^{129}\text{Xe}$  signals corresponds to an angle-random walk of  $0.0002 \text{ deg}/\sqrt{\text{hour}}$ . Better understanding of the Rb magnetometer cross-modulation peaks and short term frequency instabilities is necessary to realize the full sensitivity potential.

This work was supported by DARPA and NSF.

[1] S. K. Lamoreaux, J. P. Jacobs, B. R. Heckel, F. J. Raab, and E. N. Fortson, Phys. Rev. Lett. **57**, 3125 (1986).

- [2] M. Smiciklas, J. M. Brown, L. W. Cheuk, S. J. Smullin, and M. Romalis, *Phys. Rev. Lett.* **107** (2011).
- [3] M. Rosenberry and T. Chupp, *Phys. Rev. Lett.* **86**, 22 (2001).
- [4] C. Baker *et al.*, *Phys. Rev. Lett.* **97**, 131801 (2006).
- [5] J. M. Brown, S. J. Smullin, T. W. Kornack, and M. V. Romalis, *Phys. Rev. Lett.* **105**, 151604 (2010).
- [6] B. J. Venema, P. K. Majumder, S. K. Lamoreaux, B. R. Heckel, and E. N. Fortson, *Phys. Rev. Lett.* **68**, 135 (1992).
- [7] G. Vasilakis, J. M. Brown, T. W. Kornack, and M. V. Romalis, *Phys. Rev. Lett.* **103**, 261801 (2009).
- [8] M. Bulatowicz, R. Griffith, M. Larsen, J. Mirijanian, C. B. Fu, E. Smith, W. M. Snow, H. Yan, and T. G. Walker, *Phys. Rev. Lett.* **111**, 102001 (2013).
- [9] K. Tullney *et al.*, *Phys. Rev. Lett.* **111**, 100801 (2013).
- [10] L. Hunter, J. Gordon, S. Peck, D. Ang, and J. Lin, *Science* **339**, 928 (2013).
- [11] P. Härle, G. Wäckerle, and M. Mehring, *Applied Magnetic Resonance* **5**, 207 (1993).
- [12] E. A. Donley, in *Sensors, 2010 IEEE* (2010) pp. 17–22.
- [13] J. Kitching, S. Knappe, and E. A. Donley, *IEEE Sensors Journal* **11**, 1749 (2011).
- [14] E. Donley and J. Kitching, “Nuclear magnetic resonance gyroscopes,” (in *Optical Magnetometry*, Cambridge University Press, 2013) pp. 369–386.
- [15] D. Meyer and M. Larsen, *Gyroscopy and Navigation* **5**, 75 (2014).
- [16] T. Walker and M. Larsen, *Adv. Atom. Molec. Opt. Phys.*, **65**, 373 (2016).
- [17] D. Sheng, A. Kabcenell, and M. V. Romalis, *Phys. Rev. Lett.* **113**, 163002 (2014).
- [18] W. Makulski, *Magnetic Resonance in Chemistry* **53**, 273 (2015).
- [19] W. H. Z. Wu and J. M. Daniels, *Phys. Rev. Lett.* **59**, 1480 (1987).
- [20] V. Flambaum, S. Lambert, and M. Pospelov, *Phys. Rev. D* **80**, 105021 (2009).
- [21] S. R. Schaefer, G. D. Cates, T.-R. Chien, D. Gonatas, W. Happer, and T. G. Walker, *Phys. Rev. A* **39**, 5613 (1989).
- [22] M. V. Romalis and G. D. Cates, *Phys. Rev. A* **58**, 3004 (1998).
- [23] Z. L. Ma, E. G. Sorte, and B. Saam, *Phys. Rev. Lett.* **106**, 193005 (2011).
- [24] T. E. Chupp, R. J. Hoare, R. L. Walsworth, and B. Wu, *Phys. Rev. Lett.* **72**, 2363 (1994).
- [25] C. Gemmel *et al.*, *Phys. Rev. D* **82**, 111901 (2010).
- [26] I. M. Savukov and M. V. Romalis, *Phys. Rev. A* **71**, 023405 (2005).
- [27] J. C. Allred, R. N. Lyman, T. W. Kornack, and M. V. Romalis, *Phys. Rev. Lett.* **89**, 130801 (2002).
- [28] A. Korver, R. Wyllie, B. Lancor, and T. G. Walker, *Phys. Rev. Lett.* **111**, 043002 (2013).
- [29] See supplemental material at journals.aps.org for additional information on pulsed magnetometer and comagnetometer diagnostics and pulse-design analysis using average Hamiltonian theory, which includes Ref. [39–41].
- [30] J. K. Stockton, J. M. Geremia, A. C. Doherty, and H. Mabuchi, *Phys. Rev. A* **69**, 032109 (2004).
- [31] O. Alem, K. L. Sauer, and M. V. Romalis, *Phys. Rev. A* **87**, 013413 (2013).
- [32] F. J. Adrian, *Journal of Chemical Physics* **120**, 8469 (2004).
- [33] D. Suter, G. C. Chingas, R. A. Harris, and A. Pines, *Molecular Physics* **61**, 1327 (1987).
- [34] D. Suter, K. T. Mueller, and A. Pines, *Physical Review Letters* **60**, 1218 (1988).
- [35] S. Appelt, G. Wäckerle, and M. Mehring, *Phys. Rev. Lett.* **72**, 3921 (1994).
- [36] S. Appelt, G. Wäckerle, and M. Mehring, *Zeitschrift für Physik D Atoms, Molecules and Clusters* **34**, 75 (1995).
- [37] A. Korver, D. Thrasher, M. Bulatowicz, and T. G. Walker, *Phys. Rev. Lett.* **115**, 253001 (2015).
- [38] A. G. Glenday, C. E. Cramer, D. F. Phillips, and R. L. Walsworth, *Phys. Rev. Lett.* **101**, 261801 (2008).
- [39] M. V. Romalis, D. Sheng, B. Saam, and T. G. Walker, *Phys. Rev. Lett.* **113**, 188901 (2014).
- [40] U. Haeberlen and J. S. Waugh, *Phys. Rev.* **175**, 453 (1968).
- [41] C. Lee, D. Suter, and A. Pines, *Journal of Magnetic Resonance* (1969) **75**, 110 (1987).